Yrast transition strengths and band structure of ^{75}Br

L. Lühmann, M. Debray,* K. P. Lieb, W. Nazarewicz,† and B. Wörmann
II. Physikalisches Institut, Universität Göttingen, D-3400 Göttingen, Federal Republic of Germany

J. Eberth and T. Heck
Institut für Kernphysik der Universität zu Köln, D-5000 Köln, Federal Republic of Germany
(Received 31 October 1984)

High spin states in ^{75}Br were investigated in the reactions ^{62}Ni(^{16}O,p2n) and ^{66}Zn(^{12}C,p2n). By means of $\gamma\gamma$- and γ-neutron multiplicity coincidence measurements, rotational bands of both parities were extended up to 7 MeV excitation energy and spin $I=\frac{33}{2}$. The lifetimes of 17 yrast states were determined with the recoil distance and Doppler shift attenuation methods; the spin dependence of the side feeding time was also measured. The data have been analyzed in terms of the Strutinsky-Bogolyubov cranking model with a Woods-Saxon average potential. The first crossing observed in the negative parity bands is attributed to the alignment of a $g_{9/2}$ proton pair; the next irregularity which is also observed in the positive parity band is interpreted as the alignment of $g_{9/2}$ neutrons. The coexistence of prolate and oblate configurations at low spin and the change of nonaxial deformation with rotational frequency due to the polarization of the even-even core by the odd particle are discussed. The signature inversion visible in the negative parity bands as well as the changes in the signature splitting and reduction of $B(E2)$ values at high spins may be related to a transition from $\gamma<0°$ to $\gamma>0°$ triaxial shapes.

I. INTRODUCTION

Recent studies of high spin states in medium mass nuclei near neutron number $N=40$ by means of heavy ion fusion evaporation reactions have revealed various interesting and sometimes unexpected features of these nuclei:[1–17] very large quadrupole deformations, triaxial shapes, rapid variations of the moment of inertia as a function of angular momentum and mass number, coexistence of states with different deformations even at low spins, and band crossing phenomena associated with spin alignment of $g_{9/2}$ proton and neutron pairs. The rich spectroscopy has stirred considerable theoretical efforts to test nuclear models in this mass region.

Our motivations of the present detailed study of states and transitional moments in ^{75}Br were based on several previous findings in this nucleus and neighboring isotones:

(1) In their recent investigations of yrast states in ^{75}Br with α-particle- and oxygen-induced reactions, Winter *et al.*[13] and Kreiner *et al.*[14] have proposed two rotational bands with negative parity and a third one with positive parity, the latter one connected with a rotationally aligned $g_{9/2}$ proton. Such decoupled proton bands are common in these odd-A nuclei:[4–8] Lifetime measurements have indicated that in few cases, i.e., ^{77}Br and ^{81}Rb (Refs. 4 and 5), the $g_{9/2}$ proton acts as a spectator without disturbing the respective even-even core. In many other cases with $N\leq 40$, like in ^{69,71,73}As and ^{79}Rb (Refs. 6–8), the valence particle drives the core into a larger deformation. The onset of this polarization effect is $N=40$; ^{75}Br may therefore be a good candidate to test this property.

(2) In spite of their large quadrupole moments, the ground state bands in ^{72,74}Se and ^{74,76}Kr seem to already have mixed intrinsic structures at low spin values.[9,11] The ground state bands of ^{76}Se and ^{78}Kr, on the other hand, follow a normal rotational pattern at least up to $I^{\pi}=10^{+}$ (Refs. 10 and 12). As ^{75}Br is an isotone to ^{74}Se and ^{76}Kr, one may ask whether the odd particle "feels" the possible coexistence of the neighboring even-even isotones or whether it stabilizes one or the other shape of the core. We expect that the measurement of level energies and $E2$ transition probabilities will help in answering this question.

(3) Dramatic changes in signature splitting and electromagnetic transition rates before and after the $g_{9/2}$ band crossing have been recently observed in rotational bands in ^{76}Br and $^{81-83}$Kr (Refs. 15–17). These variations have been attributed to the γ-polarization effect of aligned quasiparticles. As both even-even cores of ^{75}Br, i.e., ^{74}Se and ^{76}Kr, are calculated to be γ soft, one may expect to observe in the spectrum of ^{75}Br some characteristic features associated with the presence of nonaxial deformation.

(4) Among the theoretical interpretations of decoupled bands in this mass region, the asymmetric rotor plus quasiparticle model,[18] the interacting boson fermion model,[19,20] and the cranked shell model[21] have been applied. These models predict different behavior of level energies and electromagnetic transition probabilities at high spins. Experimentally, one finds that the $B(E2)$ values at high spin in most nuclei studied so far in this mass region are either constant or even decrease.[8,10,11] The reason for this effect has not yet been fully understood.

Although the present investigation, preliminary results of which have been communicated in Ref. 22, aims mostly to the measurement of nuclear lifetimes by means of the Doppler shift attenuation and recoil distance methods, several other techniques including the measurement of $\gamma\gamma$

and nγ coincidences have been employed to extend the level scheme of ^{75}Br. In order to interpret the experimental findings, we used the Woods-Saxon Strutinsky-Bogolyubov cranking model employed previously in the study of low and high spin properties of some selected $A \cong 80$ nuclei.[23,24]

II. EXPERIMENTAL METHODS AND RESULTS

The experiment has been performed with the 45—65 MeV ^{16}O and 35—55 MeV ^{12}C beams of the HVEC FN tandem accelerator of the University of Cologne. High spin states in ^{75}Br were populated in the reactions ^{62}Ni(^{16}O,p2n) and ^{66}Zn(^{12}C,p2n); in both reactions, the (p2n) channel dominates in the decay of the ^{78}Kr compound nucleus. Enriched targets, several hundred μg/cm^2 thick and evaporated onto thin Au and Ta backings, were used. The beam current was typically 20—70 charge nA. A survey of experimental methods is given in Table I. As most measuring techniques and data reduction methods are standard and have been described previously,[12,25] we mention here only those details where improvements have been accomplished or which are particularly relevant in the present investigation.

A. Excitation functions, and nγ- and $\gamma\gamma$-coincidence measurements

In order to find out appropriate bombarding energies for populating states in ^{75}Br, we measured excitation functions of the γ-ray yields of known transitions in ^{75}Br (Refs. 13 and 14). Two Ge(Li) detectors of 12—20% efficiency and having energy resolutions of 1.8—2.1 keV at 1.33 MeV were positioned at 0° and 90° to the beam. Gamma ray intensities were measured in 5 MeV steps from 45 to 65 MeV beam energy and normalized relative to the intensity of the 301 keV line in ^{181}Ta emitted after Coulomb excitation of the target backing. Excitation functions of the prominent lines in ^{75}Br are displayed in Fig. 1.

Besides γ-ray singles spectra, neutron gated γ-coincidence spectra were recorded simultaneously. Neutrons were detected in a large solid angle NE 213 liquid scintillator[26] divided in four separate segments and mounted on top of the target chamber. Gamma rays in coincidence with onefold neutron events were accumulated separately. These nγ-coincidence spectra do not contain lines and Compton background from Coulomb excitation and inelastic scattering, charged particle evaporation channels (mostly ^{73}As+αp, ^{76}Se + 2p, in the present target-projectile combination), and β-decay processes. Besides having the virtues of reduced line density and background, the onefold and twofold neutron gated γ-ray spectra allow one to discriminate between exit channels in which one neutron is emitted, e.g., ^{76}Br + pn, ^{73}Se+αn, ^{72}As+αpn, ^{75}Se + 2pn, and those channels where two or more neutrons are emitted. The effect of this neutron multiplicity filter is illustrated in Fig. 2.

New transitions in ^{75}Br were established in a $\gamma\gamma$-coincidence experiment at 60 MeV oxygen energy. Three Ge(Li) detectors were placed at 0° and ±90° to the beam; all possible twofold coincidence events were recorded in a list mode and stored on magnetic tape. By setting gates in each detector, a total of six coincidence matrices containing some 250 million events was constructed off line. All coincidence spectra from the different gate detectors were usually added in order that the highest yrast transitions could be identified.

Table II summaries the level and transition energies and the relative intensities of the lines attributed to ^{75}Br, including the results of Refs. 13 and 14. The energy and intensity calibrations were done with ^{226}Ra and ^{152}Eu sources.[27] Due to the high density of lines in the 0.7—1.2 MeV range and the Doppler broadenings of the lines above 0.9 MeV, only the strong transitions up to 0.9 MeV were analyzed in the γ-ray singles spectra taken at 60 MeV beam energy and $\theta = 55°$. The relative intensities of the weaker transitions were deduced from the neutron gated spectra and the $\gamma\gamma$-coincidence data summed over all coincident gates in all detector combinations. The proposed yrast spectrum of ^{75}Br is displayed in Fig. 4. Our results complement and partially confirm the work of Kreiner *et al.*[14] and of Winter *et al.*[13] In comparison

TABLE I. Survey of measurements performed to study the levels in ^{75}Br.

Type of experiment	Reaction; beam energy	Target; backing	Positions of detectors
Excitation function of singles and neutron gated γ rays	^{62}Ni(^{16}O,p2n); 45—65 MeV ^{66}Zn(^{12}C,p2n); 35—55 MeV	570 μg/cm^2; Au 370 μg/cm^2; Ta	0°,90° 0°,90°
$\gamma\gamma$ coincidences and DSA line shapes	^{62}Ni(^{16}O,p2n); 60 MeV	300 μg/cm^2; Ta	0°,±90°
Recoil distance	^{62}Ni(^{16}O,p2n); 56 MeV	1.06 μm self-supporting	0°,55°,125°
Anisotropy of angular distribution	^{62}Ni(^{16}O,p2n); 60 MeV	260 μg/cm^2; Ta	0°, 90°, 125°; monitor: 125°

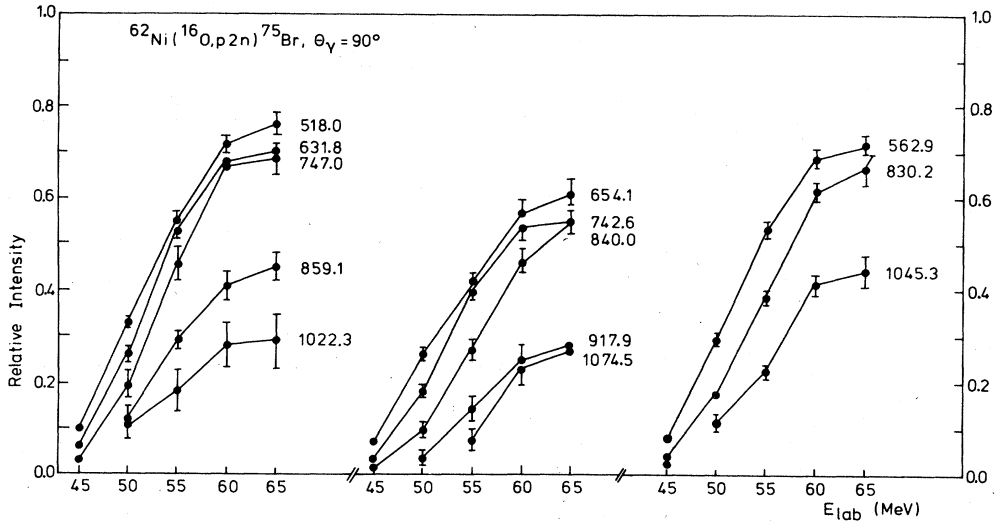

FIG. 1. Excitation functions of transitions in ^{75}Br produced in the reaction ^{62}Ni(^{16}O,p2n) and normalized to the yield of the 301 keV transition in ^{181}Ta following Coulomb excitation in the target backing.

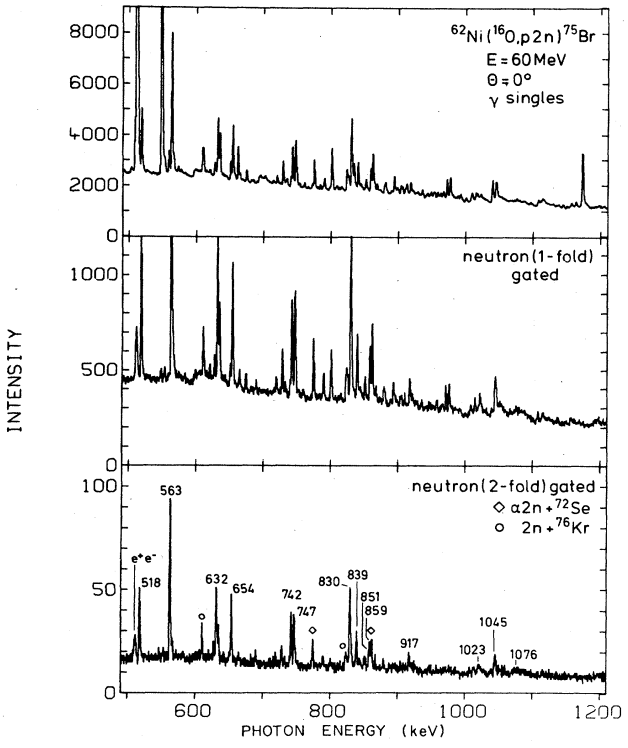

FIG. 2. Gamma ray singles and onefold and twofold neutron gated spectra taken at 60 MeV beam energy and $\theta = 0°$. In the twofold neutron gated spectrum (bottom), the dominant 2n channels ^{75}Br + p2n, ^{72}Se + α2n, and ^{76}Kr + 2n are indicated.

with the latter investigation in which the reaction ^{74}Se(^{3}He,pn)^{75}Br had been used, we disagree on the level ordering of the $\frac{3}{2}^-$ band. Winter *et al.*[13] had attributed the 631 keV line to the $2^+ \rightarrow 0^+$ transition in ^{74}Se emitted after inelastic ^{3}He scattering on the target. Inspection of the respective coincidence spectrum [see Fig. 3(b)] clearly proves that the 631.8 keV transition is part of this band.

Several small branches connecting low spin states and many new presumed yrast transitions have been identified. When summing all spectra with gates set on transitions within the positive parity favored band [Fig. 3(d), $\pi = +$, $\alpha = \frac{1}{2}$], two more Doppler broadened transitions of 1545 and 1614 keV are visible. Their energy spacings and intensities fit well on to the top of this band and suggest even higher states at 7170 keV ($\frac{37}{2}^+$) and 8984 keV ($\frac{41}{2}^+$). On the negative parity side, two weak transitions of 1390 keV [Fig. 3(a)] and 1399 keV [Fig. 3(b)] show up, but again their tentative placings on top of these bands remain doubtful.

The tentative spin-parity assignments given in Fig. 4 and Table II are based on the smooth variation of the transition energies, the 0°/90° intensity ratios, and the regular decrease of the nuclear mean lives (see the following) which are consistent with stretched, highly collective $E2$ transitions. None of the bands is intersected or strongly fed by low energy, long lived transitions, at least in the range of the energies ($E_\gamma \geq 150$ keV) and lifetimes ($\tau \leq 1$ ns) covered in the present experiment.

B. Recoil distance lifetime measurements

The mean lives of states up to 2.8 MeV excitation were obtained from a recoil distance experiment performed at a 56 MeV oxygen energy. A self-supporting ^{62}Ni foil, 1.1 μm thin, was prepared by vacuum evaporation. It was mounted in our plunger apparatus[28] and stretched to a flatness of about 1 μm as checked under a microscope.

TABLE II. Level and γ-ray energies, intensities, 0/90 intensity ratios, and mean lives of high spin states in ^{75}Br.

E_x (keV)	I^π	E_γ (keV)	Y_γ (%)[a]	$W(0)/W(90)$	τ (ps)	$B(E2,I\rightarrow I-2)(e^2\text{fm}^4)$
132.5(2)	$\frac{5}{2}^+$	132.5(2)			8.1(6) ns[b]	
220.7(2)	$\frac{9}{2}^+$	88.23(7)			38(3) ns[c]	1650(130)
373.8(2)	$\frac{7}{2}^+$	153.12(5)			82(7)	
		219.4(3)				
		241.3(3)				810(70)
783.7(3)	$\frac{13}{2}^+$	562.93(16)	100.0(14)	1.53(5)	6.8(6)	2065(175)
939.6(3)	$(\frac{11}{2})^+$	565.79(14)	10.9(6)	1.52(8)	6.6(13)	1190^{+300}_{-200}
		718.90(13)	8.6(9)	1.31(13)		
1613.9(3)	$(\frac{17}{2})^+$	830.23(7)	83.0(21)	1.57(9)	1.2(2)	1725^{+345}_{-250}
1791.4(4)	$(\frac{15}{2})^+$	851.82(23)	12.7(9)	1.51(37)		
		1008.1(7)	5(2)			
2659.2(3)	$(\frac{21}{2})^+$	1045.33(12)	53.9(12)		0.48(6)	1365^{+195}_{-150}
2863.9(6)	$(\frac{19}{2}^+)$	1072.5(4)	8.0(11)			
3868.6(4)	$(\frac{25}{2})^+$	1209.4(3)	31.7(7)		0.23(3)	1375^{+205}_{-160}
4016.7(8)	$(\frac{23}{2}^+)$	1152.8(6)	<6			
5188.9(6)	$(\frac{29}{2})^+$	1320.2(5)	16.4(10)		0.33(15)[d]	>425
6624.8(9)	$(\frac{33}{2}^+)$	1435.9(6)	10(2)			
0	$\frac{3}{2}^-$					
119.50(5)	$\frac{5}{2}^-$	119.50(5)			2.5(4) ns[c]	
518.05(2)	$\frac{7}{2}^-$	518.05(2)	43.0(11)	1.45(9)	14.7(10)	1155(90)
		398.54(3)	8.0(8)	0.39(3)		
		297.5(2)	4.5(6)	0.57(11)		
773.6(1)	$\frac{9}{2}^-$	654.13(2)	45.0(16)	1.54(9)	5.7(6)	995^{+110}_{-90}
		255.57(13)	2.3(8)			
		552.61(16)	6.9(8)			
1149.85(4)	$\frac{11}{2}^-$	631.80(4)	46.4(14)	1.50(7)	3.9(7)	2005^{+410}_{-300}
		376.23(13)	1.8(10)			
1516.2(1)	$(\frac{13}{2})^-$	742.59(9)	39.2(14)	1.44(8)	1.3(4)	2780^{+1240}_{-650}
1896.9(1)	$(\frac{15}{2})^-$	747.01(7)	39.0(17)	1.49(8)	1.8(9)	1850^{+1660}_{-595}
2356.2(2)	$(\frac{17}{2})^-$	839.99(5)	29.9(11)	1.53(18)	1.2(3)	1955^{+540}_{-330}
2755.9(1)	$(\frac{19}{2})^-$	859.05(9)	26.8(10)	1.64(25)	1.2(3)	1460^{+500}_{-300}
3274.1(2)	$(\frac{21}{2})^-$	917.91(7)	16.4(10)		0.74(10)	1695^{+430}_{-290}
3778.2(3)	$(\frac{23}{2})^-$	1022.3(2)	18.6(11)		0.54(11)	1360^{+300}_{-230}
4348.7(9)	$(\frac{25}{2})^-$	1074.6(8)	13.7(9)		0.43(5)	1325^{+260}_{-180}
4967.7(5)	$(\frac{27}{2}^-)$	1189.5(4)	12.2(10)		0.26(5)	1320^{+400}_{-250}
5601.2(10)	$(\frac{29}{2}^-)$	1252.6(4)	10.7(8)		0.20(10)[d]	>880
6231.7(11)	$(\frac{31}{2}^-)$	1264(1)	8.8(11)		0.30(15)[d]	
6932.8(11)	$(\frac{33}{2}^-)$	1331.5(5)	4.8(5)			

[a]Relative γ-ray yields measured at $\theta=55°$ and 60 MeV beam energy.
[b]From Ref. 30.
[c]From Ref. 13.
[d]Effective value, not corrected for cascade and side feeding.

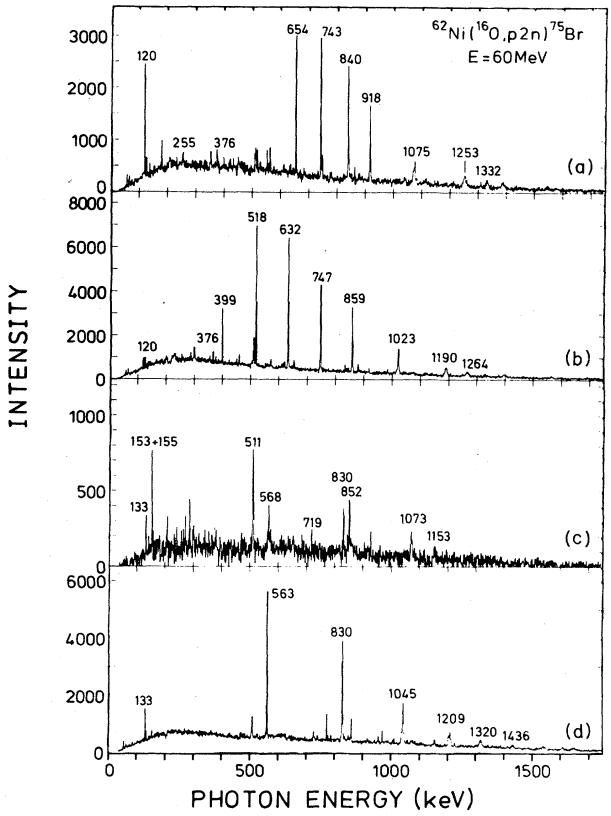

FIG. 3. Summary of twofold $\gamma\gamma$ coincidence spectra taken at 60 MeV and summed over all six combinations between the three detectors and all gates within the respective bands: (a) $\pi=-1$, $\alpha=\frac{1}{2}$; (b) $\pi=-1$, $\alpha=\frac{1}{2}$; (c) $\pi=+1$, $\alpha=-\frac{1}{2}$; (d) $\pi=+1$, $\alpha=\frac{1}{2}$.

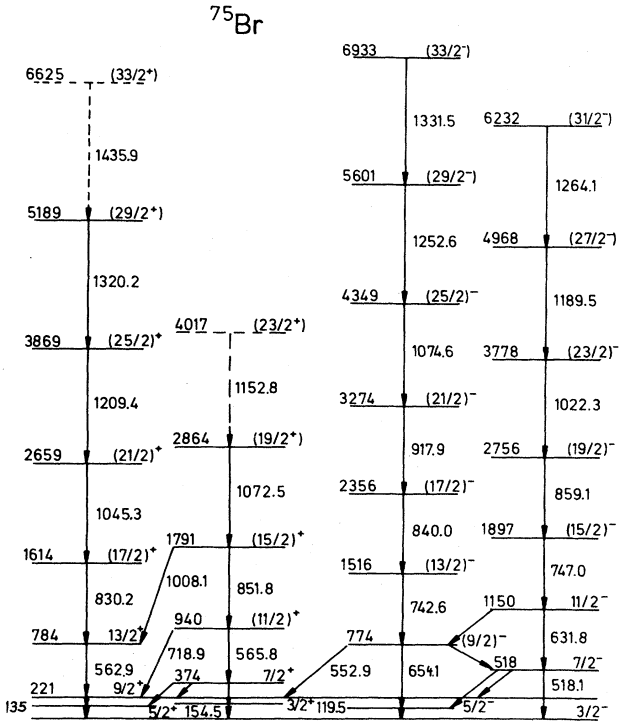

FIG. 4. Proposed level scheme of ^{75}Br.

The beam and the evaporation residues were stopped in a parallel, stretched 20 μm thick Ta foil. The recoil velocity $v/c=1.204(12)\%$ was determined from the energy differences between the stopped and Doppler shifted components of the strong ^{75}Br transitions. The simultaneous adjustment and monitoring of the recoil distance D by a micrometer screw, a magnetic transducer, and the capacitance method have been described previously.[28,29] The typical variation of the distance during a run of 1—2 h is of the order ±1 μm, while the drift of the distance zero point over a two days run is of the order of 5 μm, provided the system is kept at constant temperature (±1 °C) and under constant beam current.

Gamma ray singles spectra were taken in three Ge(Li) detectors at 0°, 55°, and 125° to the beam for about 20 recoil distances between $D=0$ (electrical contact between stopper and target foil) and $D=1$ mm. By analyzing the intensity of the stopped and Doppler shifted component normalized to the total beam charge collected individually for all three detectors, many independent measurements of all lifetimes were achieved. The measurement at forward and backward angles also allowed us to resolve the doublets in the 700—900 keV region.

A typical sample of survival ratios of the stopped component of six transitions is shown in Fig. 5. Details of the analysis, like normalization, precise determinations of zero distance, effects of hyperfine deorientation, and feeder transitions, have been fully described in previous publications;[6,25] the computer code CRONOS was used. Apart from the very lowest states which are fed by many feeders, the feeding pattern is quite simple as stretched $\Delta I=-2$ transitions prevail in all four bands and interconnecting stretched dipole transitions from states above 1.8 MeV have not been observed (Fig. 4).

Moreover, the lifetimes were found to decrease smoothly for increasing spin value. Therefore, it was sufficient to consider the next or next two transitions in each cascade, the relative intensities of which had been deduced from the 55 MeV ($\theta_\gamma=55°$) point of the excitation function in γ-ray singles and the onefold neutron gated mode. The measured lifetimes are also summarized in Table II, together with the results of the Doppler shift attenuation (DSA) analysis and the previous nanosecond lifetime measurements.[13,30]

C. DSA lifetime measurements

The excellent statistics of the 0° coincidence spectra gated with all coincident transitions in the $\pm90°$ spectra enabled us to analyze the Doppler broadened line shapes via the DSA technique. In the present case of high beam energy, high line density, and large recoil velocity, the use of coincidence data was mandatory in order to resolve details

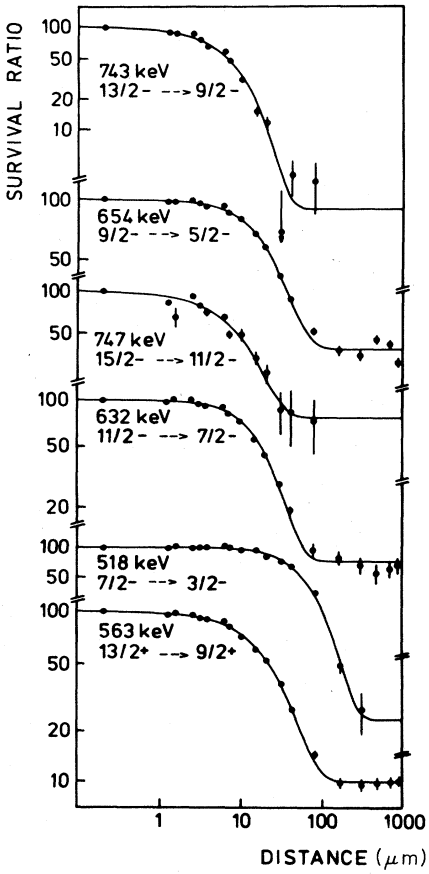

FIG. 5. Normalized intensity of stopped component (survival ratio) of several yrast transitions in ^{75}Br measured at 56 MeV beam energy and $\theta=0°$.

of the line shapes, especially for transitions from long lived states ($\tau\cong 1$ ps). In the onefold neutron gated spectra, at $\theta=0°$, which often combine good statistics, sufficiently clear Doppler profiles, and separation of the lines, the tails of the ^{75}Br doublets at 830–840, 851–859, 1008–1022, and 1072–1074 keV, respectively, overlapped and precluded a DSA analysis of these spectra.

The coincident line shapes which are shown in Fig. 6 were fitted with an improved version of the program GNOMON.[25,31] The analysis accounts for the finite target thickness (stopping of the beam and recoil nuclei), the spread of the recoil velocity both in angle and magnitude due to the evaporation kinematics, and the finite solid angle and line width of the Ge(Li) detector. Moreover, complex feeding patterns with up to five direct and cascade feeding components can be handled. In the present analysis, the spread of the recoil velocity was approximated by a Monte Carlo calculation of the reaction ^{65}Cu(^{16}O,p2n)^{78}Kr at 58 MeV.[12] Concerning the stopping power functions of the electronic and nuclear slowing down process, we adopted the semiempirical expressions proposed by Braune[32] and by Kalbitzer and Oetzmann,[33] respectively.

A more direct calibration of the stopping power parameters would be a comparison of lifetimes accessible to the DSA and recoil distance Doppler shift (RDDS) methods. In the present study, lifetimes of the 1614 keV $\frac{17}{2}^+$, 2356 keV $(\frac{17}{2})^-$, and 2756 keV $(\frac{19}{2})^-$ states turned out to be in the 0.8–1.5 ps range. The respective DSA values, $\tau=1.0(2)$, 1.0(2), and 0.9(2) ps, are systematically smaller than the RDDS values, $\tau=1.6(4)$, 1.7(4), and 1.6(4) ps although they agree in all cases within the error bars. These unusually large errors of the RDDS results are due to the serious problems of unfolding the 830-840-854-859 keV multiplets in the spectra. Lacking a more stringent test, we did not scale the electronic stopping power to achieve full agreement. For comparison, the line shapes were also analyzed with the commonly used Lindhard-Scharff-Schiøtt (LSS) ansatz;[34] the resulting lifetime values are $\tau=0.61(12)$, 0.70(13), and 0.56(10) ps, respectively, and thus in disagreement with the RDDS values. It is interesting to note that by increasing the stopping power, one also reduces the effective lifetimes of the feeder transitions and thus increases the lifetimes values deduced from the plunger measurement. Under more favorable conditions, the comparison of DSA and RDDS lifetime values is thus a fairly precise method to fix the stopping power function.

The clear Doppler profiles of the coincident 0° spectra and the simple feeding patterns of the higher yrast states also gave detailed information on the continuum (side) feeding time τ_F in this reaction. As an example, Fig. 7 illustrated fits to the line shape of the 1045 keV $(\frac{21}{2})^+ \rightarrow(\frac{17}{2})^+$ transition assuming $\tau_F=0$, 0.12 ps (best fit) and 0.3 ps. The state lifetime τ was varied until χ^2 was minimized. The deduced values of τ_F are plotted in Fig. 7 versus the excitation energy E_x and parametrized by the expression $\tau_F(\text{fs})=270-56E_x$. Side feeding times adopted in the analysis of the lower states are also indicated. The uncertainty of τ_F at lower energy is counterbalanced by the much weaker side feeding intensities of these states.

Comparable feeding times have been previously found in oxygen-induced reactions in this mass region[9] and have been well explained by Monte Carlo calculations of the evaporation and cooling down process (Refs. 9, 25, and 35). It appears that these long stretched collective yrast cascades near $N=40$ offer particularly favorable conditions to study this quantity in more detail as a function of the projectile mass and energy.

A summary of all lifetimes measured in this nucleus, the $B(E2)$ values deduced from them, the measured branching ratios,[13] and conversion coefficients is presented in the last two columns of Table II.

III. INTERPRETATION

A. Cranked shell model analysis of the experiment

The high spin spectrum of ^{75}Br proposed in Fig. 4 appears as a regular sequence of four stretched $E2$ bands reaching at least up to $I^\pi=\frac{33}{2}^\pm$. In both negative parity bands, seven stretched quadrupole transitions have been identified. We recall that, apart from the states up to $I^\pi=\frac{11}{2}^-$, no dipole transitions connecting these bands have been observed.

In order to interpret the bands of ^{75}Br the cranked shell

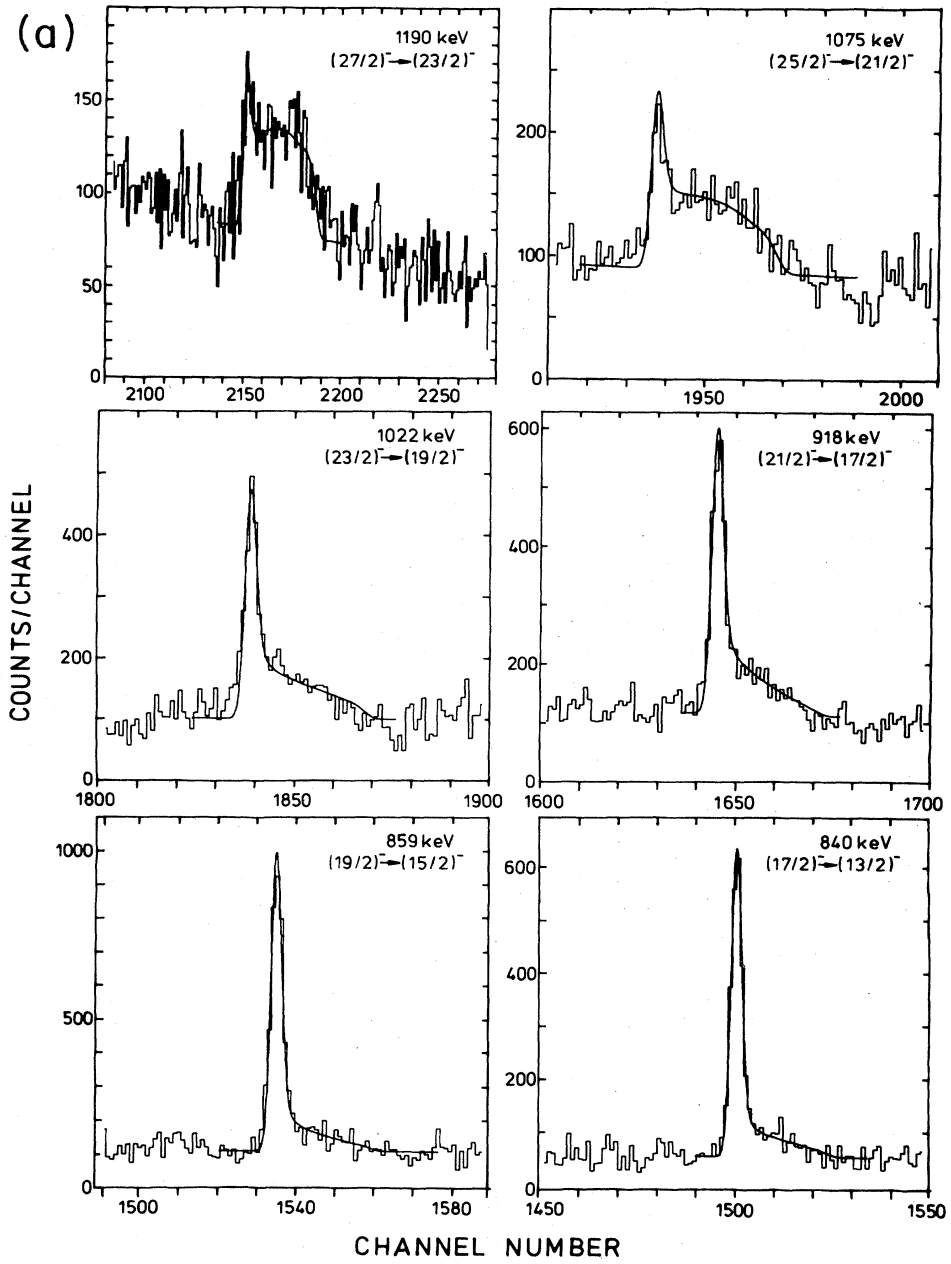

FIG. 6. Doppler broadened line shapes measured at $\theta=0°$ with coincident gates set into the two 90° detectors: (a) the negative parity 1190-1022-859 keV and 1075-918-840 keV bands; (b) the positive parity 1209-1045 cascade.

model (CSM) (Ref. 21) has been employed. Figure 8(a) shows experimental Routhians (energies in the rotating frame of reference) of measured bands in ^{75}Br versus rotational frequency. The choice of the reference curve causes some problems. The ground state band of ^{74}Se core is disturbed at low spin by the interaction with the isomeric 0_2^+ band.[10] At higher spins ($I \gtrsim 6$) the $g_{9/2}$ proton pair aligns gradually[24] leading to the upbending at $\hbar\omega \gtrsim 0.45$ MeV. Therefore the ground band of ^{74}Se can hardly be used as a reference. The same argument also applies to the second core, ^{76}Kr, where shape coexistence effects disturb the ground state band at low spins.[11] To fix a reference curve we thus used the higher spin part of the ^{76}Kr yrast band ($I \geq 4^+$).[11]

The positive parity yrast states in ^{75}Br follow the pattern of a rotationally aligned $g_{9/2}$ proton band. As in neighboring nuclei, the signature splitting between the favored ($\alpha=\frac{1}{2}$) and unfavored ($\alpha=-\frac{1}{2}$) members is very large. In the negative parity $K=\frac{3}{2}$ band the $\alpha=\frac{1}{2}$ member, which is lower in energy at low rotational fre-

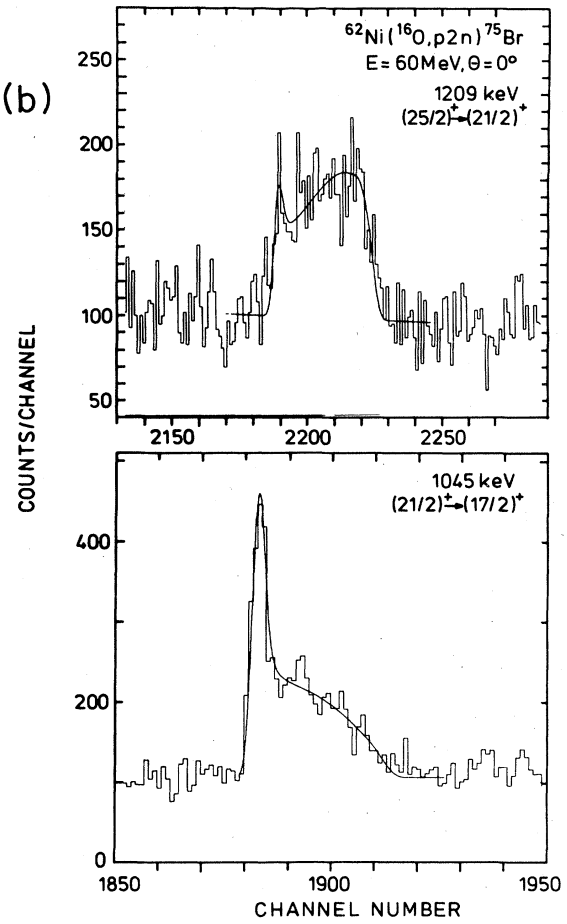

FIG. 6. (*Continued*).

quencies, crosses the $\alpha=-\frac{1}{2}$ member at $\hbar\omega\approx 0.38$ MeV (signature inversion). After this crossing the signature splitting is reduced and a next signature inversion is expected to occur at $\hbar\omega\approx 0.7$ MeV. The corresponding spin alignment plot is shown in Fig. 8(b). The aligned angular momenta for the $\pi g_{9/2}$ bands are $i_{\alpha=1/2}\approx 2.8\hbar$ and $i_{\alpha=-1/2}\approx 1.5\hbar$. The crossing with the three-quasiparticle configurations is visible in these bands at $\hbar\omega\approx 0.6$ MeV (for $\alpha=\frac{1}{2}$) and $\hbar\omega\approx 0.55$ MeV ($\alpha=-\frac{1}{2}$). The negative parity ($f_{5/2},p_{3/2}$) bands have a very small spin alignment at low rotational frequencies. It increases gradually in the frequency range 0.3 MeV $\lesssim\hbar\omega\lesssim$ 0.4 MeV approaching $i\simeq 4\hbar$. This value is very close to the alignment of the $\pi g_{9/2}^2$ band ($i\approx 4.3\hbar$), and thus suggests an explanation of this smooth upbending as a gradual $g_{9/2}$ proton alignment. This crossing does not show up in the $\pi g_{9/2}$ bands, of course, due to the blocking effect. Like in the $\pi g_{9/2}$ bands, the next crossing in the negative parity bands starts at $\hbar\omega\gtrsim 0.6$ MeV. We will interpret this upbending in Sec. III B 2 as caused by neutron $g_{9/2}$ alignment. An upbending at $\hbar\omega\approx 0.6$ MeV is also observed in ^{76}Kr (the last experimental point is, however, tentative). It can hardly be explained as a $g_{9/2}$ neutron alignment, but the shift of the crossing frequency towards higher rotational frequencies is around 200 keV when going from ^{75}Br to ^{76}Kr. We will return to this problem in Sec. III B 2.

Figure 9 shows the measured transition quadrupole moments Q_t of the rotational bands in ^{75}Br as a function of $\hbar\omega$. They were extracted from the $B(E2)$ transition rates by means of the strong coupling rotational formula

$$B(E2,I\to I-2)=\frac{5}{6\pi}\langle IK20\,|\,I-2K\rangle^2 Q_t^2 \qquad (1)$$

assuming $K=\frac{1}{2}$ and $\frac{3}{2}$ for positive and negative parity bands, respectively. The value of $K=\frac{1}{2}$ for $\pi=+$ bands accounts for the strong signature splitting indicating large admixture of the $K=\frac{1}{2}$ component in the wave function. The values of Q_t are of the order 2.0—2.5 e b and indicate large quadrupole deformations $0.28\lesssim\beta_2\lesssim 0.35$. The transition moments in the negative parity bands are reduced at low spins. They increase gradually approaching a maximum at $\hbar\omega\approx 0.4$ MeV and then start to decrease again. Nonetheless, the magnitude of this reduction is not sufficiently precise due to the experimental problems discussed in Sec. II C.

B. Theoretical interpretation

In order to draw more definite conclusions we performed cranking calculations with the Woods-Saxon potential. For more details and basic references concerning the Woods-Saxon potential and the configuration dependent Strutinsky method used, we refer the reader to Ref. 23 where the theoretical analysis of the high spin behavior in some selected $A\sim 80$ nuclei was presented in detail. We should only mention here that the Woods-Saxon potential employed there with "universal" parameters of Ref. 36 had previously been used with much success for the description of collective and single-particle properties of nuclei throughout the full periodic table.[37,38]

In Sec. III B 1 we discuss the shape coexistence effects at low spins in ^{75}Br and present the results of Strutinsky cranking calculations without inclusion of pairing correlations. In Sec. III B 2 the alignment processes in rotational bands of ^{75}Br and possible influence of nonaxiality are studied.

1. *Shape coexistence effects in ^{75}Br*

In many $A\approx 80$ even-even nuclei, coexisting 0^+ and 2^+ states, corresponding to very different deformations, have been found (Refs. 2, 9, 11, and 39). The shape coexistence is most obvious in the $N=38$ and 40 isotones of Ge, Se, and Kr. As a result of the interaction between coexisting states, the low-spin members of the ground state band do not correspond to one fixed shape but they can be treated as a mixture of well deformed (prolate) and weakly deformed (spherical or oblate) structures.[9,11]

Both even-mass neighbors of ^{75}Br, i.e., ^{74}Se and ^{76}Kr, are well known as very good examples of shape isomerism.[10,11] Figures 10(a) and (b) show the calculated energy surfaces (with inclusion of pairing) for ^{74}Se and ^{76}Kr. In

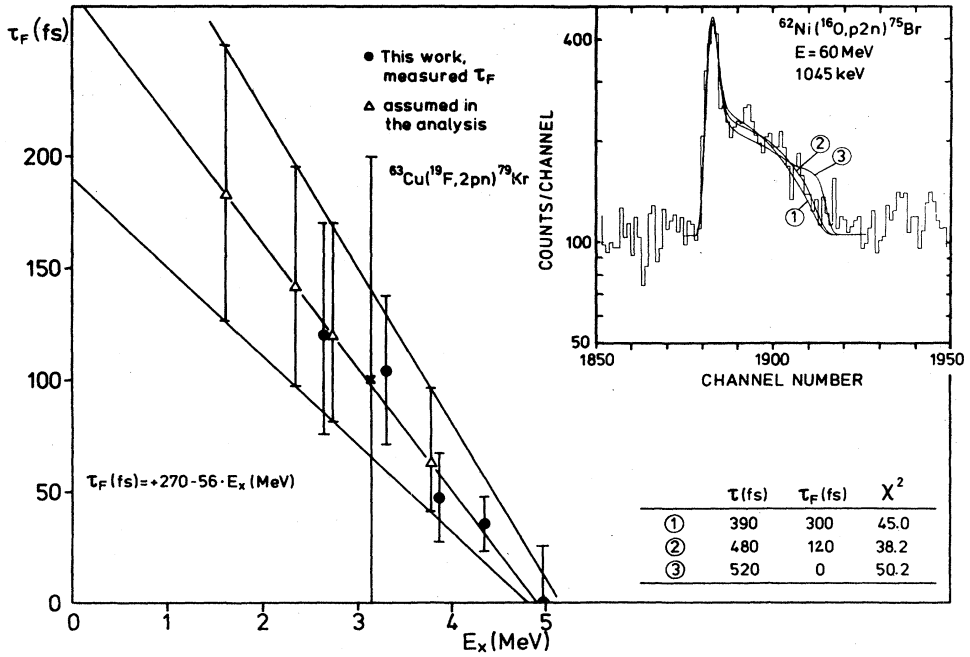

FIG. 7. DSA fits to the line shape of the 1045 keV transition for different side feeding times $\tau_F = 0$, 120 (best fit), and 300 fs. The left-hand side shows a summary of side feeding times as a function of the excitation energy E_x. Triangles denote values of τ_F used in the lifetime analysis of lower states. The point labeled ^{65}Cu(^{16}O,2pn)^{79}Kr is from Ref. 8.

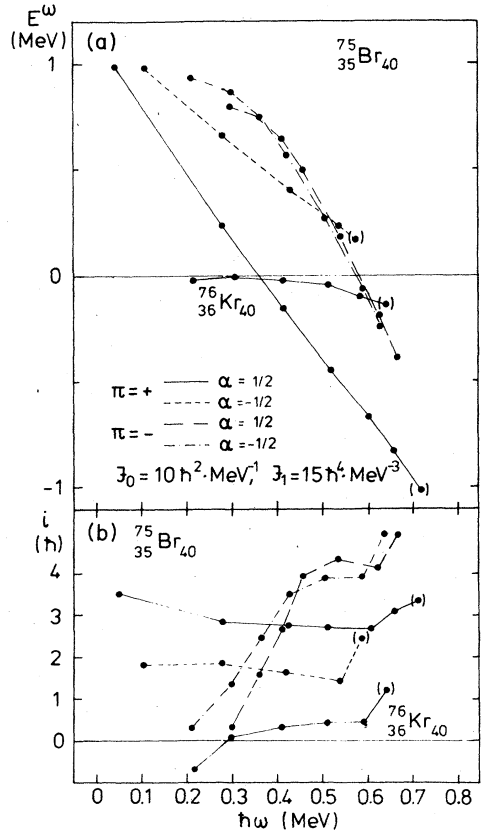

FIG. 8. Cranked shell model analysis of the band structures of ^{75}Br and ^{76}Kr.

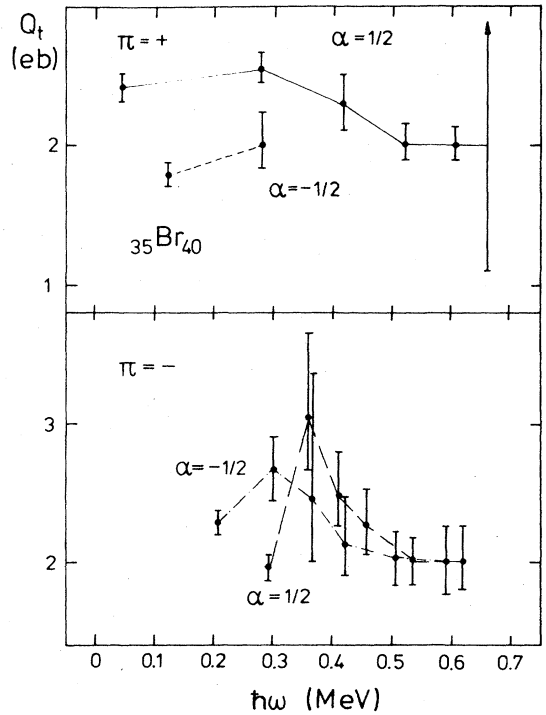

FIG. 9. Quadrupole transition moment Q_t as a function of the rotational frequency $\hbar\omega$ for rotational bands in ^{75}Br. The lines connect Q_t values within individual bands (see Fig. 8).

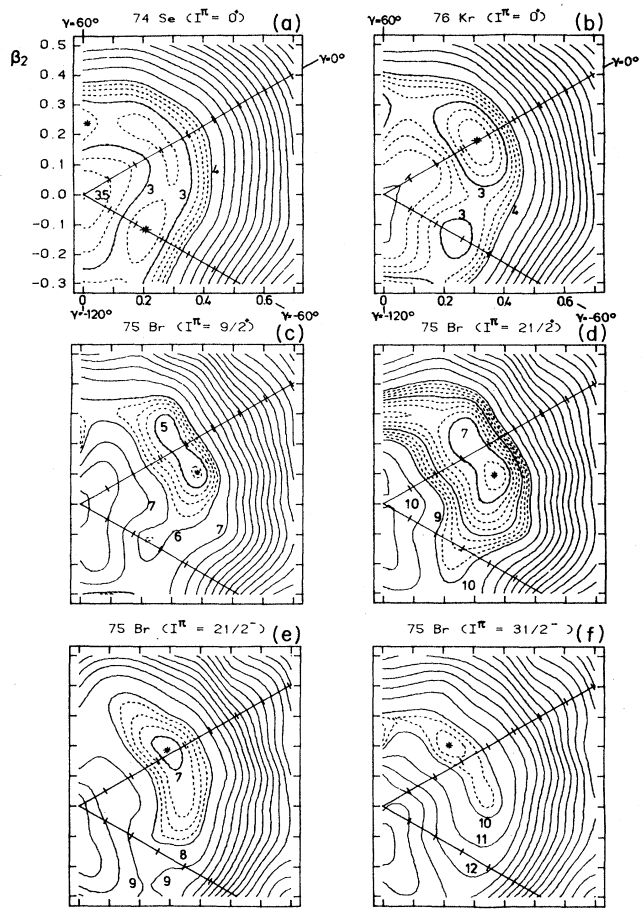

FIG. 10. Calculated total energy surfaces for ^{74}Se and ^{76}Kr at $I^\pi=0^+$ and for ^{75}Br at $I^\pi=\frac{9}{2}^+$, $\frac{21}{2}^+$, $\frac{21}{2}^-$, and $\frac{31}{2}^-$. Pairing has been included only at $I^\pi=0^+$. The energy separation between the solid lines is 1 MeV, and that between the dashed contour lines is 250 keV. The definition of the (β,γ) plane follows the Lund convention.

both cases two minima in the potential energy are present (one prolate and one oblate). The ground state of ^{74}Se has, in our calculation, oblate deformation $\beta_2=0.25$, $\gamma=-60°$, and the deformed prolate minimum with $\beta_2=0.31$, $\gamma=0°$ lies about 200 keV above the ground state. This result agrees with the conclusion of Hamilton *et al.*[9] that the ground state of ^{74}Se corresponds to a weakly deformed shape, but that the excited 0^+ state at 854 keV has a large prolate deformation. The potential energy surface for ^{74}Se is very soft in the γ direction. One can expect that rotational excitations will enhance and stabilize a well deformed minimum at high spins which is indeed observed in the experiment and reproduced by calculations.[24] The variation of the $B(E2)$ values in the ground state band of ^{74}Se deviates strongly from rigid rotation.[10] With respect to the $4^+\rightarrow2^+$ transition strength, the $2^+\rightarrow0^+$ and $6^+\rightarrow4^+B(E2)$ values are considerably suppressed, which can be traced to shape isomerism (in the 0^+ and 2^+ states) and $g_{9/2}$ proton alignment at $I\geq6^+$ (see Ref. 24).

When going to the other $N=40$ core of ^{75}Br, namely ^{76}Kr, the situation changes slightly. The prolate minimum at $\beta_2=0.35$, $\gamma=0°$ is 550 keV below the oblate one with $\beta_2=0.35$, $\gamma=-60°$ (see also Ref. 40). This result is consistent with the observed large deformation for the ground state band of ^{76}Kr and smaller deformation of the 770 keV state.[11] The potential energy surface for ^{76}Kr is still soft in the γ direction, but not as much as the one for ^{74}Se.

In order to get some idea about the deformation parameters of the 1 qp states and the changes which may occur in the yrast lines in ^{75}Br, we first calculated the potential energy surfaces for a number of low-lying configurations without considering pairing correlations. The results are presented in Figs. 10(c)–(f) for the $I^\pi=\frac{9}{2}^+$, $\frac{21}{2}^+$, $\frac{21}{2}^-$, and $\frac{31}{2}^-$ yrast configurations. In all cases the calculated equilibrium deformations are near-prolate with $0.32\lesssim\beta_2\lesssim0.37$. However, like in ^{74}Se and ^{76}Kr, the energy landscapes are flat in the γ direction and the resulting equilibrium γ values are in the range $-10°\lesssim\gamma\lesssim+10°$, depending on configuration and angular momentum. The existence of a second oblate minimum at $I^\pi=\frac{9}{2}^+$ is worth noticing.

In detailed investigations the pairing correlations must, of course, be included. Based on the results of Fig. 10 we can restrict ourselves to limited regions of the deformation space in which we know from the calculations without pairing that the selected configurations will be energetically favored. This procedure has practically been justified in Ref. 23 in the analysis of the ^{80}Sr spectrum and it has recently been employed to other $A\simeq80$ nuclei.[24] In order to see whether the shape coexistence is also present in ^{75}Br we have calculated the deformations and energies of the low-lying band heads. Triaxial shapes have not been considered in the analysis of band heads and we cannot exclude the possibility of triaxiality. The energy of the one-quasiparticle state ν, characterized by K and π quantum numbers,

$$E_\nu(\beta_2,\beta_4)=E_{\rm LD}(\beta_2,\beta_4)+\delta E_{{\rm shell},\nu}(\beta_2,\beta_4)+\delta E_{{\rm pair},\nu}(\beta_2,\beta_4)\ , \qquad (2)$$

was calculated using the usual Strutinsky method[41] with the Woods-Saxon potential and the macroscopic energy, $E_{\rm LD}$, was assumed to be of the form of liquid drop.[42] The pairing correction term $\delta E_{{\rm pair},\nu}$ was computed employing the standard Bardeen-Cooper-Schrieffer (BCS) treatment with blocking.

The energies of one-quasiparticle states of ^{75}Br plotted versus β_2 are shown in Fig. 12. At each value of β_2 ($\gamma=0°$) the energy (2) has been minimized with respect to the hexadecapole degree of freedom β_4. The β_4 values are usually very close to zero and therefore not displayed in Fig. 11. At spherical shape ($\beta_2=0$) states are labeled by spherical quantum numbers (l,j). The calculated bandhead energies, deformations, and wave functions are summarized in Table III together with existing experimental data. The calculations reproduce the experimentally observed level order. The ground state band head is calculated to be $\frac{3}{2}^-$ and the next excited state is $\frac{3}{2}^+$. Both of

TABLE III. Low-lying experimental levels and theoretical band head energies of ^{75}Br, labeled by K^π. The quadrupole deformations β_2 and dominant components of the wave functions are also given.

E_{exp} (keV)	E_{th} (keV)	K^π	β_2	Configuration
0	0	$\frac{3}{2}^-$	+0.33	$0.82\,\|f_{5/2}\rangle+0.35\,\|p_{3/2}\rangle+\cdots$
154.5	40	$\frac{3}{2}^+$	+0.35	$0.81\,\|g_{9/2}\rangle+\cdots$
	150	$\frac{1}{2}^+$	+0.30	$0.73\,\|g_{9/2}\rangle-0.36\,\|d_{5/2}\rangle+\cdots$
	80	$\frac{9}{2}^+$	−0.26	$0.94\,\|g_{9/2}\rangle+\cdots$
(179.3)[a] (273.1)[b]	240	$\frac{1}{2}^-$	+0.35	$0.61\,\|p_{3/2}\rangle-0.59\,\|f_{5/2}\rangle+\cdots$
	400	$\frac{1}{2}^-$	−0.25	$0.66\,\|f_{5/2}\rangle-0.58\,\|p_{3/2}\rangle+\cdots$
	560	$\frac{3}{2}^-$	−0.19	$0.91\,\|f_{5/2}\rangle+\cdots$

[a] $I^\pi=(\frac{1}{2}^-)$, Ref. 13.
[b] $I^\pi=(\frac{1}{2}^-,\frac{3}{2}^-)$, Ref. 13.

them have large prolate deformations. The other three low-lying single-particle states, $\frac{9}{2}^+$, $\frac{1}{2}^-$ (at 400 keV), and $\frac{3}{2}^-$ (at 560 keV) are predicted to have oblate deformations. As can be seen from Table III, the positive parity states have a dominating $g_{9/2}$ component, although the $d_{5/2}$ admixture to the $K^\pi=\frac{1}{2}^+$ orbital is clearly present. The negative parity states have dominating $f_{5/2}$ and $p_{3/2}$ components.

The $\frac{3}{2}^-$ ground state (prolate) has a very similar structure as the $\frac{3}{2}^-$ (oblate) excited state. The overlap between their single-particle wave functions is

$$\langle \tfrac{3}{2}^-,\beta_2=0.33\,|\,\tfrac{3}{2}^-,\beta_2=-0.19\rangle\approx 0.8 \qquad (3a)$$

(cf. Table III). The same is true for the $\frac{1}{2}^-$ (prolate) and $\frac{1}{2}^-$ (oblate) states:

$$\langle \tfrac{1}{2}^-,\beta_2=0.35\,|\,\tfrac{1}{2}^-,\beta_2=-0.25\rangle\approx 0.75\ . \qquad (3b)$$

The interaction between the (1qp) states ν_{prol} and ν_{obl} in the odd-mass nucleus can be approximately given as

$$\langle \nu_{prol}\,|\,V\,|\,\nu_{obl}\rangle=\langle \text{core}_{prol}\,|\,V\,|\,\text{core}_{obl}\rangle x\langle \nu_{prol}\,|\,\nu_{obl}\rangle\ , \qquad (4)$$

where $\langle \text{core}_{prol}\,|\,V\,|\,\text{core}_{obl}\rangle$ is the effective interaction between the ground state and the 0_2^+ isomeric state of the even-even core (calculated as one-half of the sum of experimentally deduced interactions in both even-even neighbors). Both the $\frac{3}{2}^-$ and $\frac{1}{2}^-$ prolate states have their structural analogs on the oblate side and the corresponding rotational bands will be then disturbed at low spins due to the interaction with the oblate-deformed orbitals. The reduction of Q_t in the negative parity bands in ^{75}Br observed at low spins (Fig. 9) may therefore be explained in the same way as the reduction of $B(E2,2^+\rightarrow 0^+)$ values in ^{74}Se and ^{76}Kr (Ref. 10 and 11), i.e., in terms of the prolate-oblate band mixing. On the other band, the low-K positive parity $g_{9/2}$ prolate states have no structural analogs on the oblate side, where the high-K $g_{9/2}$ orbitals are present (see Fig. 11). The shape coexistence effects in these $g_{9/2}$ bands are thus expected to be rather weak.

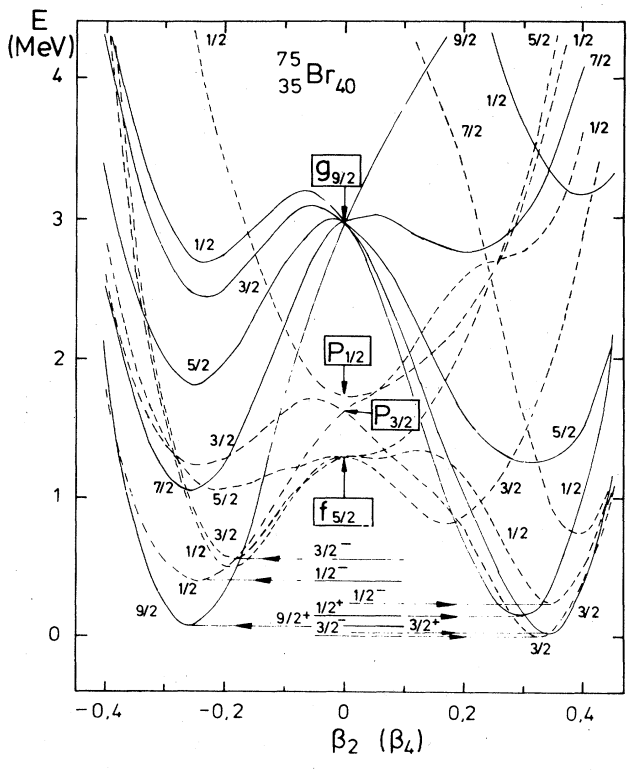

FIG. 11. The total energy of the one-quasiparticle states in ^{75}Br calculated with the Woods-Saxon potential. The solid lines correspond to positive parity states and the dashed lines to negative parity states.

2. Deformation changes and band crossing at high spins

In order to discuss the possible deformation changes caused by the aligned odd particles we employ the simple method proposed in Ref. 43 which has been applied to study the interplay between the single-particle and shape degrees of freedom in γ-soft nuclei (Refs. 16, 43–46). We write the total Routhian of an n-quasiparticle configuration as

$$E^{\omega}(\gamma)=E_g^{\omega}(\gamma)+\sum_{L=1}^{n} E_L^{\omega}(\gamma)\ , \tag{5}$$

where $E_g^{\omega}(\gamma)$ is the vacuum reference and E_L^{ω} are the quasiparticle Routhians. The reference Routhian E_g^{ω} was computed according to the formula

$$E_g^{\omega}(\gamma)=V_{\rm Str}(\gamma)+\langle H^{\omega}\rangle-\langle H^{\omega}\rangle\,|_{\omega=0} \tag{6}$$

in which the Strutinsky potential $V_{\rm Str}$ was calculated as one-half of the sum of the Strutinsky potentials of ^{74}Se and ^{76}Kr. The even-odd mass difference reflects not only the energy of pair correlations, but also the contribution connected with deformation effects. The pairing gap values for these nuclei can therefore be hardly determined from the even-odd mass differences, as their deformations change rapidly from the nucleus and shape isomerism is also present.

We therefore employed the BCS Δ values[23] which (at $\omega=0$) are $\Delta_p\approx 1.1$ MeV and $\Delta_n\simeq 1.5$ MeV for almost all low-lying one-quasiparticle states in ^{75}Br. The further reduction ($\Delta_p=1.0$ MeV, $\Delta_n=1.4$ MeV) accounts for the weaker pair field at higher rotational frequencies. The reduced value of the proton pairing Δ_p is consistent with the frequency of the first $\pi g_{9/2}$ crossing at 0.38 MeV (see Fig. 8 and the following discussion). The quadrupole deformation was fixed to $\beta_2=0.35$ (see Figs. 10 and 11) and the rotational frequency to $\hbar\omega=0.40$ MeV. The equilibrium deformation was then determined by minimization of the total Routhian $E^{\omega}(\gamma)$ with respect to γ.

In Fig. 12 the lowest calculated 1qp Routhians for protons ($Z=35$) and neutrons ($N=40$) are plotted as a function of γ. It is seen that the (1qp) proton excitations have different γ-driving tendencies. The gamma deformation of the favored $g_{9/2}$ band ($\alpha=\frac{1}{2}$, $\pi=+$) is mainly determined by the minimum of the reference, as the $(\frac{1}{2},+)$ Routhian is very flat in the γ plane. The $g_{9/2}$ $(-\frac{1}{2},+)$ and negative parity $(-\frac{1}{2},-)$ excitations favor positive γ values, while the $(\frac{1}{2},-)$ excitation drives the core towards $\gamma<0°$. Apart from the γ driving forces of the excited quasiparticles an additional force comes from the core. At $\hbar\omega=0.4$ MeV, the calculated equilibrium γ values of the negative parity band are close to $\gamma=0°$, namely $\gamma=-5°$ $(+\frac{1}{2},-)$ and $\gamma=+1°$ $(-\frac{1}{2},-)$ before the $g_{9/2}$ proton alignment, and $\gamma=-2°$ $(+\frac{1}{2},-)$ and $\gamma=+8°$ $(-\frac{1}{2},-)$ after the proton alignment. This estimate then shows the tendency of a spin aligned proton pair to drive the system towards $\gamma>0°$ deformation. We emphasize the agreement between the above estimate and the calculations without pairing presented in Fig. 10: The $\frac{9}{2}^+$ and $\frac{21}{2}^+$ yrast states of the unpaired ($\alpha=\frac{1}{2}$, $\pi=+$) band have both $\gamma<0°$; the $\frac{21}{2}^-$ state of the $(\frac{1}{2},-)$ band has $\gamma\approx 0°$ and the $\frac{31}{2}^-$ configuration of the $(-\frac{1}{2},-)$ band has a positive γ value, respectively. The $g_{9/2}$ two-quasineutron excitation has a maximum at $\gamma\approx 0°$ [Fig. 12(b)] and an equally strong γ-driving tendency both into the $\gamma>0$ and $\gamma<0$ areas.

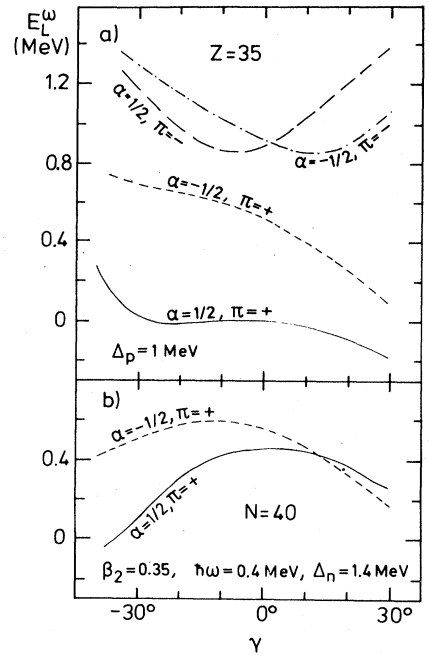

FIG. 12. Energies of lowest quasiparticle Routhians plotted vs γ at $\beta_2=0.35$ and $\hbar\omega=0.4$ MeV for $Z=35$ and $N=40$. Note the signature inversion in the proton negative parity Routhians at $\gamma=0°$ and the neutron $g_{9/2}$ Routhians at $\gamma=13°$.

We now discuss the frequency dependence of the quasiparticle Routhians at fixed values of β_2 and γ. Figure 13 shows proton quasiparticle Routhians for $\beta_2=0.32$, $\gamma=-4°$ representative below the first band crossing, while Fig. 13(b) shows them for $\beta_2=0.32$, $\gamma=+7°$ representative above the first band crossing. Both diagrams show that there must be a large interaction between the 1qp and the 3qp configurations in the proton system leading to the gradual $\pi g_{9/2}$ alignment observed in the experiment. Both the crossing frequency $\hbar\omega_c=0.4$ MeV, the $g_{9/2}$ spin alignments ($i_{\alpha=1/2}=2.9\hbar$, $i_{\alpha=-1/2}=1.5\hbar$), and the signature splitting agree well with the corresponding experimental values [see Figs. 8(b) and 13(a) and (b)]. When going from $\gamma<0°$ to $\gamma>0°$, the signature order of the lowest negative parity proton Routhians is predicted to change in accordance with experiment [see Fig. 8(a)]. The observed signature inversion and change of signature splitting can therefore be related to the variation of the γ deformation of the core induced by the polarization effect to the two $g_{9/2}$ quasiparticle protons. The next signature inversion in the negative parity bands should occur near $\hbar\omega=0.7$ MeV [see Fig. 13(b)], which is in line with the extrapolated trend of the data [see Fig. 8(a)]. The neutron

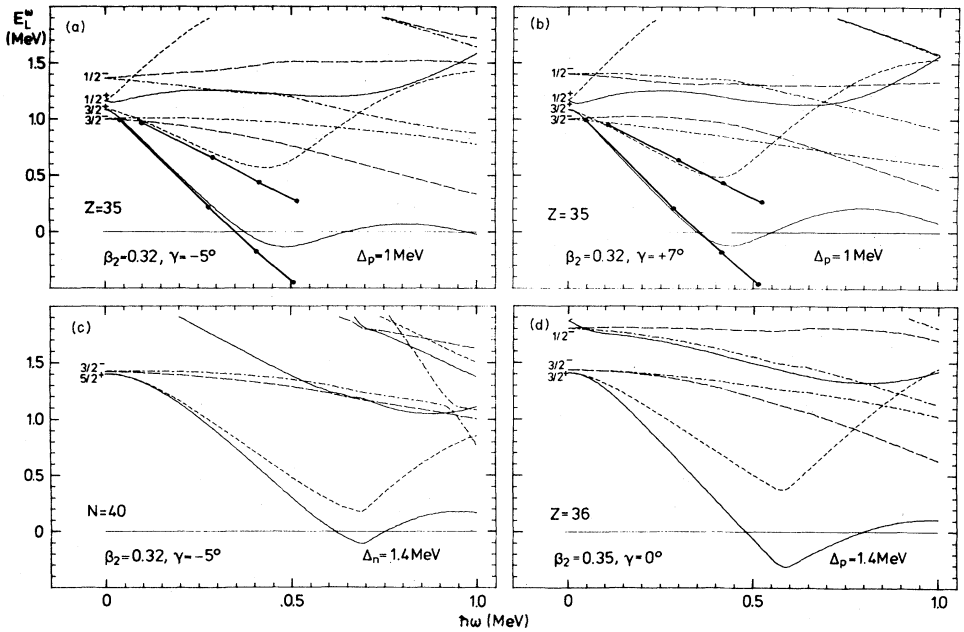

FIG. 13. Quasiparticle Routhians of the protons (a) and (b) and of the neutrons (c) in ^{75}Br and of the protons in ^{76}Kr (d). The signature and parity of the individual levels are indicated in the same way as in Fig. 8. The levels are labeled with the K value (although K is not a good quantum number for $\gamma \neq 0°$ and $\hbar\omega > 0$). The experimental $g_{9/2}$ Routhians are marked by dots.

$N=40$ quasiparticle Routhians are shown in Fig. 13(c). The neutron crossing is expected to occur around $\hbar\omega_c = 0.65$ MeV. The irregularities observed in all bands of ^{75}Br for $\hbar\omega \gtrsim 0.6$ MeV and in the $\pi g_{9/2}$ band in ^{77}Rb at $\hbar\omega \approx 0.7$ MeV (Ref. 47) can thus be related to the $g_{9/2}$ neutron alignment. The $Z=36$ quasiparticle proton Routhians for $\beta_2=0.35$, $\gamma=0°$, which is a representative deformation for the ground state band of ^{76}Kr, are shown in Fig. 13(d). The strong proton crossing, similar to that which has recently been observed in ^{74}Kr (Ref. 48), is expected in this nucleus at frequency $\hbar\omega_c \approx 0.6$ MeV, in agreement with the observed increase in alignment for ^{76}Kr at $\hbar\omega \gtrsim 0.6$ MeV [see Fig. 8(b)]. The large odd-even variation of the $\pi g_{9/2}$ crossing frequency ($\Delta\hbar\omega_c \approx 200$ keV) for the pair ^{75}Br-^{76}Kr has also been observed by Funke *et al.*[49] to be present for the pairs ^{77}Br-^{78}Kr and ^{81}Rb-^{80}Kr. It suggests that in the considered region of nuclei the blocking due to the valence particle can reduce pairing considerably. For comparison, the odd-even variation of $\hbar\omega_c$ observed in rare-earth nuclei[50] is of the order of 50 keV. It was mentioned before that the transition moment Q_t in all bands decreases above $I=\frac{13}{2}$ (see Table II) or $\hbar\omega \gtrsim 0.4$ MeV (see Fig. 9). In the cranking approximation Q_t depends on the deformation parameters as[51]

$$Q_t(\beta_2,\gamma) = Q_t(\beta_2,\gamma=0°)\cos(\gamma+30°)2/\sqrt{3} \ . \qquad (7)$$

Therefore Q_t decreases when the nonaxial deformation changes from $\gamma<0°$ to $\gamma>0°$. The observed reduction of Q_t by 20–30 % (see Fig. 9) can thus be related to the increasing γ deformation with rotational frequency. An additional decrease of Q_t due to a small reduction of β_2 cannot be excluded (see Ref. 24 and the discussion in Ref. 52). In the negative parity bands some part of this reduction at frequency range 0.3 MeV $\lesssim \hbar\omega \lesssim$ 0.4 MeV can obviously be explained by the $(\pi g_{9/2})^2$ alignment. The larger (in average) Q_t values for the $(\frac{1}{2},-)$ band compared to that of the $(-\frac{1}{2},-)$ band may possibly be attributed to the difference between their γ parameters.

IV. CONCLUSIONS

Energies and $E2$ transition probabilities of the rotational bands of both parities and signatures in ^{75}Br have been measured in a detailed in-beam γ-spectroscopic study. Based on the spin-parity assignments made by Winter *et al.*[13] and Kreiner *et al.*,[14] the bands have been extended up to $I^\pi = \frac{33}{2}^\pm$. Lifetimes of yrast levels have been determined by the Doppler shift attenuation and recoil distance methods up to $I^\pi = \frac{29}{2}^\pm$. Due to the simple feeding pattern of these yrast cascades it has been possible to deduce the spin dependence of the continuum feeding time τ_F which was found to decrease for increasing excitation energy. Neither the energies nor the $B(E2)$ values follow the simple rotational model with constant moment of inertia and deformation parameters: all bands show several irregularities and the $B(E2)$ values decrease above $I^\pi = \frac{13}{2}^\pm$.

The experimental data on ^{75}Br have been analyzed in terms of the cranked shell model with the nonaxially deformed Woods-Saxon potential. This approach turned

out to give a consistent description of the effects observed. The main conclusions of this study and suggestions for future work are as follows:

(i) The large $B(E2)$ values indicate pronounced deformations in all bands up to the highest spins measured.

(ii) The gradual spin alignment $i \approx 4\hbar$ observed in the negative parity bands at $\hbar\omega \approx 0.4$ MeV is due to the proton $g_{9/2}$ alignment.

(iii) The irregularities in the aligned angular momentum versus the $\hbar\omega$ plot [Fig. 8(b)] observed at $\hbar\omega \approx 0.6$ MeV in all bands are caused by the neutron $g_{9/2}$ alignment. The theory predicts a sharp band crossing with $i \approx 4.8\hbar$. The extension of the experimental data for higher spins is needed to confirm this expectation.

(iv) The reduction of transition moments Q_t observed at low rotational frequencies in the negative parity bands is probably due the shape coexistence, in analogy to the $N=40$ cores ^{74}Se and ^{76}Kr. The absence of such a reduction in the $\pi g_{9/2}$ bands is due to the lack of low-K $\pi g_{9/2}$ oblate band heads at low energy. The one-quasiparticle oblate bands can be characterized by smaller moments of inertia, smaller and negative static quadrupole moments, and $E2$ transition rates considerably reduced compared to the ones observed in the prolate bands. Further experimental evidence for such structures is needed to confirm our prediction. It may be worthwhile to mention here that the shape coexistence in the odd-mass nucleus ^{81}Sr has recently been reported[53] and discussed in Ref. 23.

(v) The signature inversion observed in the negative parity bands at $\hbar\omega \approx 0.38$ MeV, the expected next signature inversion in the negative parity bands at $\hbar\omega \approx 0.7$ MeV, as well as the reduction of Q_t values at high rotational frequencies, are consistent with the predicted decrease of γ from $\gamma < 0°$ to $\gamma > 0°$.

(vi) The considerable reduction of about 400 keV in the proton pairing gap Δ_p is expected to be caused by the blocking effect. It leads to the shift in crossing frequency, $\Delta\hbar\omega_c \approx 200$ keV, which is also observed in the neighboring odd-proton nuclei.

(vii) At high rotational frequencies ($\hbar\omega \gtrsim 1$ MeV) a shape transition to triaxial configurations ($\gamma \approx 30°$) containing the aligned $h_{11/2}$ particles is expected.[23] The noncollective states corresponding to $\gamma = 60°$ are predicted to become yrast or close to yrast for $I \gtrsim \frac{89}{2}$.

ACKNOWLEDGMENTS

The authors are indebted to the tandem accelerator crew for the very good condition of the machine; to J. Panqueva and W. Neumann for their help in the initial stage of the work; and to J. Roth for setting up the neutron multiplicity filter. Discussions with R. Bengtsson are gratefully acknowledged. The potential energy calculations have been performed in collaboration with J. Dudek. This work was supported by Deutsches Bundersministerium für Forschung und Technologie and the Swedish Natural Science Research Council.

*Present address: Comision Nacional de Energia Atomica, Buenos Aires, Argentina.

†On leave of absence from Department of Mathematical Physics, Lund Institute of Technology, S-22007 Lund, Sweden.

[1]E. Nolte, Y. Shida, W. Kutschera, R. Prestele, and H. Morinaga, Z. Phys. **268**, 267 (1974).

[2]J. H. Hamilton, Lecture Notes in Physics, Vol. 168 (Springer, Heidelberg, 1982), p. 287; C. J. Lister, B. J. Varley, H. G. Price, and J. W. Olness, Phys. Rev. Lett. **49**, 308 (1982); L. V. Theisen, S. L. Tabor, L. R. Medsker, G. Neuschaefer, L. H. Fry, and S. S. Clements, Phys. Rev. C **25**, 1325 (1982).

[3]K. P. Lieb, in Proceedings of the XIX Winter School on Physics, Zakopane, 1984 (in press).

[4]H. Schäfer, A. Dewald, A. Gelberg, U. Kaup, and P. von Brentano, Z. Phys. A **293**, 85 (1979).

[5]J. Panqueva, H. P. Hellmeister, L. Lühmann, K. P. Lieb, F. J. Bergmeister, P. von Brentano, and R. Richter, Nucl. Phys. **A376**, 367 (1982).

[6]H. P. Hellmeister, E. Schmidt, M. Uhrmacher, R. Rascher, K. P. Lieb, and D. Pantelica, Phys. Rev. C **17**, 2113 (1978).

[7]B. Heits, H. G. Friedrichs, A. Gelberg, K. P. Lieb, A. Perego, R. Rascher, K. O. Zell, and P. von Brentano, Phys. Lett. **61B**, 33 (1976).

[8]J. Panqueva, H. P. Hellmeister, L. Lühmann, F. J. Bergmeister, K. P. Lieb, and T. Otsuka, Nucl. Phys. **A389**, 424 (1982).

[9]J. H. Hamilton *et al.*, Phys. Rev. Lett. **32**, 239 (1974); K. P. Lieb and J. J. Kolata, Phys. Rev. C **15**, 939 (1977).

[10]M. L. Halbert, P. O. Tjom, I. Espe, G. B. Hagemann, B. Herskind, and M. Neiman, Nucl. Phys. **A259**, 496 (1976); R. B. Piercey, A. V. Ramayya, R. M. Ronningen, J. H. Hamilton, R. L. Robinson, and H. J. Kim, Phys. Rev. Lett. **37**, 496 (1976); J. Barrette, M. Barrette, G. Lamoureux, S. Monaro, and S. Markiza, Nucl. Phys. **A235**, 154 (1974).

[11]R. B. Piercey, A. V. Ramayya, J. H. Hamilton, X. J. Sun, R. L. Robinson, H. J. Kim, and J. C. Wells, Phys. Rev. C **25**, 1941 (1982); R. B. Piercey *et al.*, Phys. Rev. Lett. **47**, 1524 (1981); B. Wörmann, K. P. Lieb, R. Diller, L. Lühmann, J. Keinonen, L. Cleemann, and J. Eberth, Nucl. Phys. **A431**, 170 (1984).

[12]H. P. Hellmeister, J. Keinonen, K. P. Lieb, U. Kaup, R. Rascher, R. Ballini, J. Delaunay, and H. Dumont, Nucl. Phys. **A332**, 241 (1979).

[13]G. Winter, J. Döring, W. D. Fromm, L. Funke, P. Kemnitz, H. Prade, and E. Will, Nucl. Phys. **A367**, 95 (1981).

[14]A. J. Kreiner, M. A. J. Mariscotti, C. Baktash, E. der Mateosian, and P. Thieberger, Phys. Rev. C **24**, 148 (1981).

[15]L. Funke, in *Proceedings of the XX International Winter Meeting on Nuclear Physics, Bormio, 1982,* edited by I. Iori (Ricerca Scientifica Educazione Permanente, Milano, 1982), p. 213.

[16]P. Kemnitz, J. Döring, L. Funke, F. R. May, P. Ojeda, E. Will, and G. Winter, Z. Phys. A **313**, 367 (1983).

[17]L. Funke, F. Dönau, J. Döring, P. Kemnitz, G. Winter, L. Hildingson, L. A. Johnson, and Th. Lindblad, Phys. Lett. **120B**, 301 (1983).

[18]F. S. Stephens, Rev. Mod. Phys. **47**, 43 (1975); H. Toki and A. Faessler, Phys. Lett. **63B**, 121 (1976).
[19]F. Iachello and O. Scholten, Phys. Rev. Lett. **43**, 679 (1979).
[20]I. Talmi, in *Interacting Bose Fermion Systems in Nuclei,* edited by F. Iachello (Plenum, New York, 1981), p. 329.
[21]R. Bengtsson and S. Frauendorf, Nucl. Phys. **A314**, 27 (1979); **A327**, 139 (1979).
[22]L. Lühmann, B. Wörmann, M. Debray, K. P. Lieb, J. Eberth, T. Heck, and W. Neumann, in *Proceedings of the International Conference on Nuclear Physics, Florence, Italy, 1983,* edited by Blasi and R. A. Ricci (Tipografia Compositori, Bologna, 1983), Vol. I, p. B52.
[23]W. Nazarewicz, J. Dudek, R. Bengtsson, T. Bengtsson, and I. Ragnarsson, Nucl. Phys. **A435**, 397 (1985).
[24]R. Bengtsson and W. Nazarewicz, in Proceedings of the XIX Winter School on Physics, Zakopane, 1984 (in press); R. Bengtsson, J. Dudek, and W. Nazarewicz (unpublished).
[25]H. P. Hellmeister, Ph.D. thesis, Universität Köln, 1980 (unpublished).
[26]J. Roth, Ph.D. thesis, Universität Köln, 1981 (unpublished).
[27]V. Zobel, J. Eberth, U. Eberth, and E. Eube, Nucl. Instrum. Methods **141**, 329 (1977).
[28]K. P. Lieb, M. Uhrmacher, J. Dauk, and A. M. Kleinfeld, Nucl. Phys. **A223**, 445 (1974).
[29]J. Panqueva, Ph.D. thesis, Universität Köln, 1982 (unpublished).
[30]E. Roeckl, D. Lode, and W. Pessara, Z. Phys. **266**, 123 (1974).
[31]L. Lühmann, Ph.D. thesis, Universität Göttingen, 1984 (unpublished).
[32]H. Braune, quoted in D. Pelte and D. Schwalm, *Heavy Ion Collisions,* edited by R. Bock (North-Holland, Amsterdam, 1982), Vol. II, p. 1ff.
[33]S. Kalbitzer and H. Oetzmann, in Proceedings of the International Conference on Ion Beam Modifications of Materials, Budapest, 1978.
[34]V. Lindhard, M. Scharff, and H. E. Schiøtt, K. Dan. Vidensk. Selsk. Mat.-Fys. Medd. **33**, No. 14 (1963).
[35]H. P. Hellmeister, K. P. Lieb, and W. F. J. Müller, Nucl. Phys. **A307**, 515 (1978).
[36]J. Dudek, Z. Szymanski, and T. Werner, Phys. Rev. C **23**, 920 (1981).
[37]M. de Voigt, J. Dudek, and Z. Szymanski, Rev. Mod. Phys. **55**, 949 (1983).
[38]G. Leander, J. Dudek, W. Nazarewicz, J. R. Nix, and P. Quentin, Phys. Rev. C **30**, 416 (1984).
[39]J. H. Hamilton, H. L. Crowell, R. L. Robinson, A. V. Ramayya, W. E. Collins, R. M. Ronningen, V. Maruhn-Rezwassi, J. A. Maruhn, N. C. Singhal, H. J. Kim, R. O. Sayer, T. Magee, and L. C. Whitlock, Phys. Rev. Lett. **36**, 340 (1976).
[40]R. Bengtsson *et al.*, Phys. Scr. **29**, 402 (1984).
[41]V. M. Strutinsky, Nucl. Phys. **A95**, 420 (1967).
[42]W. D. Myers and W. Swiatecki, Ark. Fys. **36**, 343 (1967).
[43]S. Frauendorf and F. R. May, Phys. Lett. **125B**, 245 (1983).
[44]Y. S. Chen, Nucl. Phys. **A421**, 403c (1984).
[45]Y. S. Chen, S. Frauendorf, and G. A. Leander, Phys. Rev. C **28**, 2437 (1983).
[46]G. A. Leander, S. Frauendorf, and F. R. May, in *Proceedings of the International Conference on High Angular Momentum Properties of Nuclei, Oak Ridge, 1982,* edited by N. R. Johnson (Harwood, New York, 1983), p. 281.
[47]C. J. Lister, G. B. Varley, L. Lühmann, K. P. Lieb, H. G. Price, and J. W. Olness, *Proceedings of the 7th International Conference on Atomic Masses and Fundamental Constants, Darmstadt, 1984,* edited by O. Klepper (THD Schriftenreihe zu Wissenschaft und Technik, Darmstadt, 1984), p. 300.
[48]J. Roth *et al.*, J. Phys. G **10**, L25 (1984).
[49]L. Funke, J. Döring, F. Dubbers, P. Kemnitz, E. Will, G. Winter, V. G. Kiptilij, M. F. Kudojarov, I. Kh. Lemberg, A. A. Pasternak, A. S. Mishin, L. Hildingsson, A. Johnson, and Th. Lindblad, Nucl. Phys. **A355**, 228 (1981).
[50]J. D. Garrett, O. Anderson, J. J. Gardhoje, G. B. Hagemann, B. Herskind, J. Kownacki, J. C. Lisle, L. L. Riedinger, W. Walús, N. Roy, S. Jönsson, H. Ryde, M. Guttormsen, and P. O. Tjøm, Phys. Rev. Lett. **47**, 75 (1983).
[51]A. Bohr and B. R. Mottelson, *Nuclear Structure* (Benjamin, New York, 1975), Vol. II; P. Ring, A. Hayashi, K. Hara, H. Emling, and E. Grosse, Phys. Lett. **110B**, 423 (1981).
[52]H. Emling, E. Grosse, R. Kulessa, D. Schwalm, and H. J. Wollersheim, Nucl. Phys. **A419**, 187 (1984).
[53]G. C. Hicks, C. J. Gross, U. J. Hüttmeier, Xi-Thing Lu, G. Neuschaefer, and S. L. Tabor, Phys. Rev. C **29**, 1345 (1984).